Desalination and Water Treatment
www.deswater.com
doi: 10.1080/19443994.2016.1167628

57 (2016) 27294–27313
December

Taylor & Francis
Taylor & Francis Group

Defluoridation studies with synthesized magnesium-incorporated hydroxyapatite and parameter optimization using response surface methodology

Poonam Mondal*, Dhiraj Mehta, Suja George

Department of Chemical Engineering, Malaviya National Institute of Technology Jaipur, Jaipur, Rajasthan 302017, India, emails: poonam.mbiotech@gmail.com (P. Mondal), dhiraj.mbiotech@gmail.com (D. Mehta), sujageorge.mnit@gmail.com (S. George)

Received 21 November 2015; Accepted 13 March 2016

ABSTRACT

The severe impact of consumption of excess fluoride on human health has raised concerns for development of reliable materials for defluoridation of drinking water. This study deals with the synthesis of magnesium-incorporated hydroxyapatite (M-i-HAP) and evaluation of its defluoridation potential. Characterization studies revealed the bonding patterns, phase characteristics, and other microstructural details of the adsorbent synthesized, and the surface area was found to be 46.62 m^2/g. Response surface methodology was used for optimization of fluoride adsorption on the adsorbent and development of the predictive model. The optimum conditions evaluated using central composite statistical design for fluoride removal were found to be 303 K, pH 7, 180 min contact time, and 10 g/L of M-i-HAP for treating fluoride solution of 10 mg/L. At these conditions, the actual removal experimentally achieved was 94.5% which was very close to the maximum removal predicted by the model (94.60%). The process followed pseudo-second-order kinetic model and the adsorption mechanism can be described by Langmuir isotherm with an adsorption capacity of 1.16 mg/g. The adsorbent was regenerated 91% using 0.1 M NaOH solution. Drinking water quality was assessed for various parameters and the treated water was found to be fit for consumption with all parameters such as pH, total dissolved solids, total hardness, alkalinity, and turbidity within permissible limit as per World Health Organization and Bureau of Indian Standards (BIS) guidelines.

Keywords: Adsorption; Drinking water; Fluoride; Optimization; Response surface methodology

1. Introduction

The subtle balance of fluoride needed for human body is very crucial defining the thin boundary between a beneficial element to a contaminant. Fluoride when present up to 1.0 mg/L in drinking water is beneficial for strengthening tooth enamel and avoids dental caries, while concentrations above 1.5 mg/L may lead to dental and skeletal fluorosis [1,2]. At molecular level also presence of fluoride causes various toxicological affects such as hindering cellular respiration, affecting the glucose metabolism, and initiating inflammation response [3]. Regions suffering from high fluoride concentrations are mainly located

*Corresponding author.

in rural and secluded areas in China, India, Kenya, Tanzania, Mexico, Turkey, and Ethiopia [4]. In these areas, efficient defluoridation processes such as reverse osmosis, nanofiltration and electrocoagulation are not feasible both technologically and economically. Adsorption serves best in these cases owing to the high efficiency, selectivity, and relatively low cost of the process for unraveling the problem of high fluoride content in potable water [3,5]. The diverse list of adsorbents that have been applied for reducing excess fluoride from drinking water includes activated alumina [6], calcite [5,7], montmorillonite [8], chitin, and composite [9].

In the past decade, biomaterials were being extensively used as defluoridating agents. Among them, the most promising biomaterial is Hydroxyapatite ($Ca_{10}(PO_4)_6(OH)_2$), which is a naturally occurring mineral form of calcium apatite. Adsorption of fluoride using hydroxyapatite has been reported by many researchers [5,10–14]. Some studies have shown modification of hydroxyapatite for enhanced defluoridation behavior. Nie et al. [15] incorporated aluminum into hydroxyapatite, Tomar et al. [16] dispersed nanoparticles of hydroxyapatite inside activated alumina granules to prepare a hybrid adsorbent. Hydroxyapatite has widely been used in the medical field as bone and teeth implants [17], while magnesium substituted hydroxyapatite has recently been used in bone tissue engineering as artificial bone substitutes [18,19] in view of the fact that magnesium stimulates osteoblast proliferation [20]. However, hydroxyapatite incorporated with magnesium has never been used as an adsorbent to solve water contamination issues such as defluoridation. This study is a novel approach to synthesize and utilize the biomaterial, magnesium-incorporated hydroxyapatite, for fluoride mitigation in drinking water.

Most of the adsorbents found in literature with high capacities are metal based due to which presence of residual metal ions in treated water is a major area of concern. While working with lanthanum-modified chitosan, Kamble et al. [21] stated the release of lanthanum ions (1.05 mg/L) into treated solution at alkaline pH and in the presence of other anions. Iron (1.48 mg/L) and zirconium ions (1.88 μg/L) leached into treated water from granular zirconium-ferric oxide adsorbent [22]. Aluminum ions also reportedly leached from aluminum-modified hydroxyapatite [15]. Presence of residual aluminum in treated water has been reported by many researchers [23–25], causing neurotoxicity which demands development of alternative materials for defluoridation. All these metal elements have extremely low permissible limit in drinking water as per WHO above which they are toxic to human beings, whereas calcium and magnesium possess much higher permissible limits of 75 and 30 ppm, respectively. Hence, use of magnesium-incorporated hydroxyapatite for fluoride removal will provide an added advantage of the absence of any toxic metal leaching.

Limitations of a classical experimental method can be eliminated by optimizing all the factors affecting together by statistical experimental design such as response surface methodology (RSM) [26]. RSM is mainly used for modeling of process parameters and to evaluate the relative importance of factors influencing the process even in the presence of complex interaction [27]. This methodology is widely used in chemical and environmental engineering, particularly to optimize adsorption process [28]. By utilizing RSM, response over an entire space may be examined along with locating the region where the response value reaches optimum. The intent of this study was application of RSM coupled with central composite design (CCD) as a statistic tool for optimization of fluoride adsorption using magnesium-incorporated hydroxyapatite. The equilibrium data were described with different isotherm models. The kinetic and thermodynamic parameters have also been evaluated for the adsorption process.

2. Materials and methods

2.1. Synthesis of magnesium-incorporated hydroxyapatite (M-i-HAP)

M-i-HAP was synthesized using the chemical precipitation method [18,19]. Potassium phosphate dibasic (K_2HPO_4), calcium nitrate tetrahydrate ($Ca(NO_3)_2{\cdot}4H_2O$), and magnesium nitrate hexahydrate ($Mg(NO)_3{\cdot}6H_2O$) were used as source of phosphorous, calcium, and magnesium, respectively. All the reagents used for this research work were of AR grade from E. Merck Pvt. Ltd, India.

For synthesizing M-i-HAP, 0.19 M potassium phosphate was added dropwise into an alkaline solution consisting of magnesium nitrate and calcium nitrate with varying Mg/Ca molar ratios. The solution was constantly stirred at 700–1,000 rpm at 70–80 °C. The total concentration of magnesium and calcium in initial solution was 0.32 M. Ammonia solution (NH_4OH) was used to maintain the alkalinity of solution during the reaction time. The suspension subsequently obtained was kept for aging (24 h) at room temperature. Thereafter, it was centrifuged at 2,500 rpm for 15 min and the pellet was dried in an oven at 110 °C for 5 h. The dried material was ground and the powder obtained was used as an adsorbent for batch

studies. The targeted chemical composition correspond to "n" values of 0, 1.5, 2, and 4 in the chemical formula of M-i-HAP [i.e. $Ca_{(10-n)}Mg_n(PO_4)_6(OH)_2$] and denoted as pHAP (pure hydroxyapatite), M-i-HAPa, M-i-HAPb, and M-i-HAPc, respectively. Since this formula does not consider increase in phosphate ion incorporation or the lattice defects due to increase in magnesium concentration in hydroxyapatite; therefore, it may only be used as an approximation [29]. Reaction for synthesis of M-i-HAP is presented as follows in Eq. (1):

$$(10-n)\{Ca(NO_3)_2\} + n\{Mg(NO_3)_2)\} + 6K_2HPO_4 + 8NH_4OH \rightarrow Ca_{(10-n)}Mg_n(PO_4)_6(OH)_2 + 12KNO_3 + 8NH_4NO_3 + 6H_2O \quad (1)$$

2.2. Characterization of synthesized adsorbent

FTIR studies were done for evaluating the bonding patterns in M-i-HAP in the wavenumber range of 400–4,000 cm^{-1} with a resolution of 4 cm^{-1} and the spectra were recorded on a Perkin Elmer UTR two spectrophotometer under ambient conditions. X-ray powder diffraction analysis was conducted for compositional analysis of sample in a X'pert Powder Panalytical diffractometer using Cu Kα radiation (λ = 1.5418 Å) at a scanning range of $2\theta = 10^\circ$–70° with a speed of 0.5 s and a scan step of 0.02°. The crystallographic structure of M-i-HAP was determined with transmission electron microscope (Technai G2T20). Energy dispersive X-ray spectroscopy (Xflash 6TI30 Bruker) was used to measure the elemental composition on the adsorbent surface. Further, the surface area and pore size distribution of the adsorbent were calculated from the corresponding nitrogen adsorption–desorption isotherm at 77.57 K using a Micrometrics ASAP analyzer 2010. The specific surface area was calculated using the BET isotherms, and the pore size distribution was determined using the density functional theory.

2.3. Batch adsorption experiments

Batch fluoride adsorption studies were carried out by varying adsorbent dose, pH, fluoride concentration, contact time, and temperature in the presence of interfering ions. The experiments were performed in 250-ml PVC containers with 100 ml working volume and the sample solutions with desired adsorbent concentrations were shaken at 200 ± 10 rpm at 303 ± 1 K. Equilibrium studies were carried out with M-i-HAP dose of 2–18 g/L and kinetic studies at fixed dose of 10 g/L for initial fluoride concentration of 10 mg/L. Thereafter, the aqueous solutions were filtered using a Whatman 42 filter paper and then residual fluoride concentrations were analyzed with an Ion meter (Orion Versa Star). TISAB II buffer was used for analysis and used in 1:1 ratio with fluoride samples. All the experiments were performed using double distilled water. The fluoride removal (%) and adsorption capacity (mg/g) were calculated using Eqs. (2) and (3):

$$q_e = (C_i - C_e) \times \frac{v}{w} \quad (2)$$

$$\text{Fluoride removal } (\%) = (C_i - C_e)/C_i \times 100 \quad (3)$$

Each experiment was conducted in duplicates and average values are reported. pH of the solution was measured with Orion Versa star pH meter and maintained using 0.01 M NaOH and HCl. The point of zero charge (pH_{PZC}) of the M-i-HAP was determined by the solid addition method, using 0.15 g of adsorbent with 0.01 M NaCl as a background electrolyte, whose initial pH values (2–12) were adjusted by small additions of diluted (0.01 M) HCl or NaOH. TDS, electrical conductivity (EC), and calcium leached in treated water were analyzed using respective ion meter electrodes, while turbidity present in the aqueous solution was measured with a turbidity meter (NT4000, Spectra Lab). For evaluating the total hardness, total alkalinity, and magnesium and phosphorus concentration of solution APHA standard procedures were used [30].

2.4. Design of experiments

The optimization of fluoride removal was carried out by four chosen independent process variables viz. adsorbent dose (2–18 g/L), pH (3–11), contact time (15–345 min), and temperature (303–323 K) and the response was observed in terms of fluoride removal (%) and adsorption capacity (mg/g). The response was studied with a standard RSM design called CCD. This method was selected since it is appropriate for fitting a quadratic surface and it helps optimize the effective parameters with a minimum number of experiments, and also to analyze the interaction between the parameters [31]. CCD consists of a 2^n factorial runs with 2^n axial runs, and n_c center runs (six replicates) which indicated that 30 experiments were required. These 30 experiments were performed as per the design mentioned in Table 1. Design Expert Version 9.0.4.1 (Stat Ease, USA) was used for regression and graphical analysis of the data obtained. The optimum values of the chosen parameters were acquired

Table 1
Experimental design matrix and responses for fluoride sorption using M-i-HAPa

Run	Factor 1 *A*: Adsorbent dose (g/L)	Factor 2 *B*: Temperature (K)	Factor 3 *C*: Time (min)	Factor 4 *D*: pH	Response 1 fluoride removal		Response 2 adsorption capacity	
					Observed value (%)	Predicted value (%)	Observed value (mg/g)	Predicted value (mg/g)
1	2	323	345	11	25	27.4	1.25	1.33
2	10	313	180	9	90	90.1	0.9	0.93
3	2	303	345	3	45	45.02	2.25	2.17
4	2	323	15	3	28	27.95	1.4	1.3
5	18	323	345	3	82	84.16	0.45	0.44
6	18	323	15	11	50	51.26	0.27	0.28
7	10	313	180	7	91.5	90.12	0.91	0.96
8	2	323	15	11	22	21.19	1.1	1.00
9	10	313	100	7	83	83.09	0.83	0.88
10	18	323	345	11	85	82.09	0.472	0.32
11	10	313	180	5	90	91.47	0.9	0.99
12	18	303	15	11	55	55.67	0.3	0.26
13	10	313	180	7	91	90.12	0.91	0.96
14	10	318	180	7	87	88.15	0.87	0.90
15	18	323	15	3	55	54.55	0.33	0.36
16	2	303	345	11	43.8	42.85	2.19	2.03
17	10	313	260	7	92	93.59	0.92	1.04
18	18	303	345	11	92.7	94.03	0.52	0.55
19	2	303	15	11	30	29.12	1.5	1.4
20	10	313	180	7	91	90.12	0.91	0.96
21	2	303	15	3	31	32.51	1.55	1.57
22	10	313	180	7	91	90.12	0.91	0.96
23	2	323	345	3	35	32.94	1.75	1.66
24	6	313	180	7	70	71.97	1.16	1.26
25	10	303	180	7	94.5	94.60	0.95	1.09
26	10	313	180	7	91	90.12	0.91	0.96
27	18	303	345	3	93.3	92.72	0.52	0.49
28	14	313	180	7	91.8	91.41	0.918	0.66
29	18	303	15	3	56.7	55.58	0.32	0.17
30	10	313	180	7	91	90.1	0.9	0.96

by solving the regression equation and by examining the response surface plots [32]. An empirical model was developed for correlating the response to the adsorption process and is based on a second-order quadratic model for fluoride removal using M-i-HAP as given by Eq. (4):

$$Y = b_0 + \sum_{i=1}^{n} b_i X_i + \sum_{i=1}^{n} b_{ii} X_i^2 + \sum_{i=1}^{n} \sum_{j>1}^{n} b_{ij}\ X_i X_j \qquad (4)$$

3. Results and discussion

3.1. Selection and characterization of synthesized adsorbent

The effect of magnesium incorporation on fluoride removal was evaluated as shown in Fig. 1, and M-i-HAPa showed highest removal. Therefore, it was used for all the experiments. M-i-HAPa exhibited a surface area of 46.62 m^2/g which is more than twice of pHAP (21.25 m^2/g). The pore volume and pore size of M-i-HAPa was 0.177 cm^3/g and 152.51 Å, respectively, while that of pHAP was 0.090 cm^3/g and 169.83 Å, respectively. Fig. 2 represents the nitrogen adsorption–desorption isotherm and the corresponding pore size and pore volume distributions of pHAP and M-i-HAPa, respectively.

FTIR studies were conducted for assessing the functional groups and bonding patterns in the sample, as well as to evaluate the effect of magnesium incorporation on phosphate and hydroxyl groups. As presented in Fig. 3(a), bands at 3,560 and 633 cm^{-1} corresponds to the stretching and vibrational mode of OH^- groups, respectively. The characteristic PO_4^{3-}

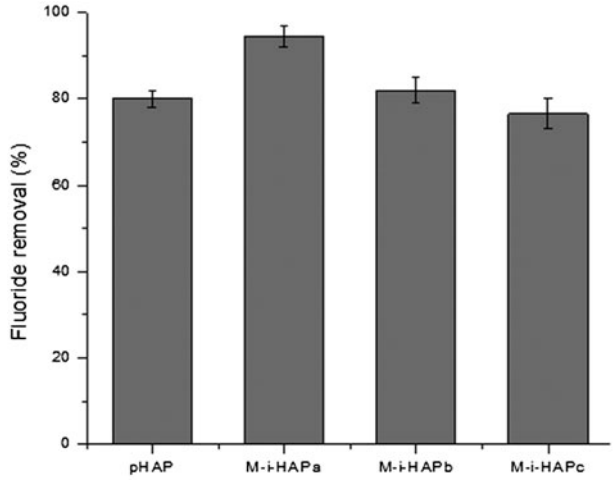

Fig. 1. Fluoride removal with different M-i-HAPs synthesized (Dose: 10 g/L, contact time: 3 h, F^-: 10 mg/L, pH 7).

bands related with hydroxyapatite were seen at 566, 633, 980, and 1,041 cm^{-1}. Precipitated powders generally have high specific surface area, due to which adsorbed water bands were spotted at 3,000–3,300 cm^{-1}. The bands observed in the range 1,470–1,410 cm^{-1} demonstrate that the CO_3^{2-} (carbonate) groups substitute phosphate in the hydroxyapatite lattice since the experiments are performed in air. Similar observations were noted by Suchanek et al. [29] and Farzadi et al. [19]. Spectra of M-i-HAP showed broadening and splitting of the characteristic PO_4^{3-} absorption bands due to the presence of magnesium.

The XRD pattern of M-i-HAPs is presented in Fig. 3(b). Hydroxyapatite peaks were distinctly observed and crystallographic identification of samples was achieved using the standards of JCPDS (Joint committee on Powder diffraction) followed by matching them with the experimental patterns obtained. All the peaks matched with card no. 09–0,432 for hydroxyapatite and a peak for MgO was observed at 2θ of 37.5° (045–0,946), demonstrating incorporation of Mg^{2+} in HAP structure. Due to the large size difference between Mg and Ca radius (~0.28 Å according to the Pauling scale) strong distortions of the hydroxyapatite lattice is observed which in turn reduces its crystallinity. TEM images as shown in Fig. 3(c) displayed elongated needle-like nanorod structure for pHAP and aggregated structures arranged in random orientations were observed for M-i-HAPs. Higher concentration of magnesium induces greater agglomeration and did not favor HAP formation. Clear reduction of grain size on incorporation of magnesium into hydroxyapatite structure is observed. Particle size estimated from TEM for pHAP is 100–150 nm in length and 15–18 nm in width. The particle size was observed to be smaller after magnesium incorporation i.e. 6–10 nm for M-i-HAPa and M-i-HAPb. Owing to cluster formation particle size for M-i-HAPc could not be estimated accurately. Due to higher agglomeration, spherical structures were noticed in TEM mage of M-i-HAPa which attributed to its higher surface area and higher fluoride removal capacity as compared to pHAP as shown in Fig. 1. The elemental composition of the adsorbents synthesized is studied through EDX and displayed in Fig. 3(d).

3.2. Effect of pH

Performance of most of the adsorbents is pH dependent which makes it an important parameter to study. The effect of pH on fluoride removal efficiency of M-i-HAPa was evaluated at pH ranging between 3 and 11. The pH_{ZPC} was depicted to be 7.5 for both pHAP and M-i-HAPa (Fig. 4). As it is evident from Fig. 5(a), there is only a slight variation in the removal efficiency with changing pH. A minor decrease in percentile adsorption of fluoride was noted at pH higher than 8 which may be due to competition by hydroxyl ions present at alkaline conditions. On the other hand, pHAP removal decreased drastically at higher pH. However, it is noteworthy that the residual fluoride concentrations using M-i-HAPa at all the pH values were below 1.0 mg/L. Thus, satisfying the permissible limits prescribed by regulatory authorities [1,2]. Since, for $pH < pH_{PZC}$ (7.5) the adsorbent surface is positive, higher fluoride adsorption is observed due to electrostatic attraction [33]. Defluoridation studies using M-i-HAPa were not affected by pH, which is an advantage over other adsorbents.

3.3. Effect of adsorbent dose

The effect of the dose of adsorbent on fluoride removal capacity was studied at fixed conditions of pH 7 for 10 mg/L initial fluoride solution and contact time of 180 min. The dose of adsorbent was varied from 2 to 18 g/L (Fig. 5(b)). At higher doses, availability of active sites for fluoride adsorption is higher and after certain limit the capacity becomes constant. It was found that 10 mg/L of M-i-HAPa was required for obtaining residual fluoride below permissible limit (<1.0) [2].

3.4. Effect of contact time

On conducting studies varying contact time of adsorbent in fluoride solution of fixed concentration

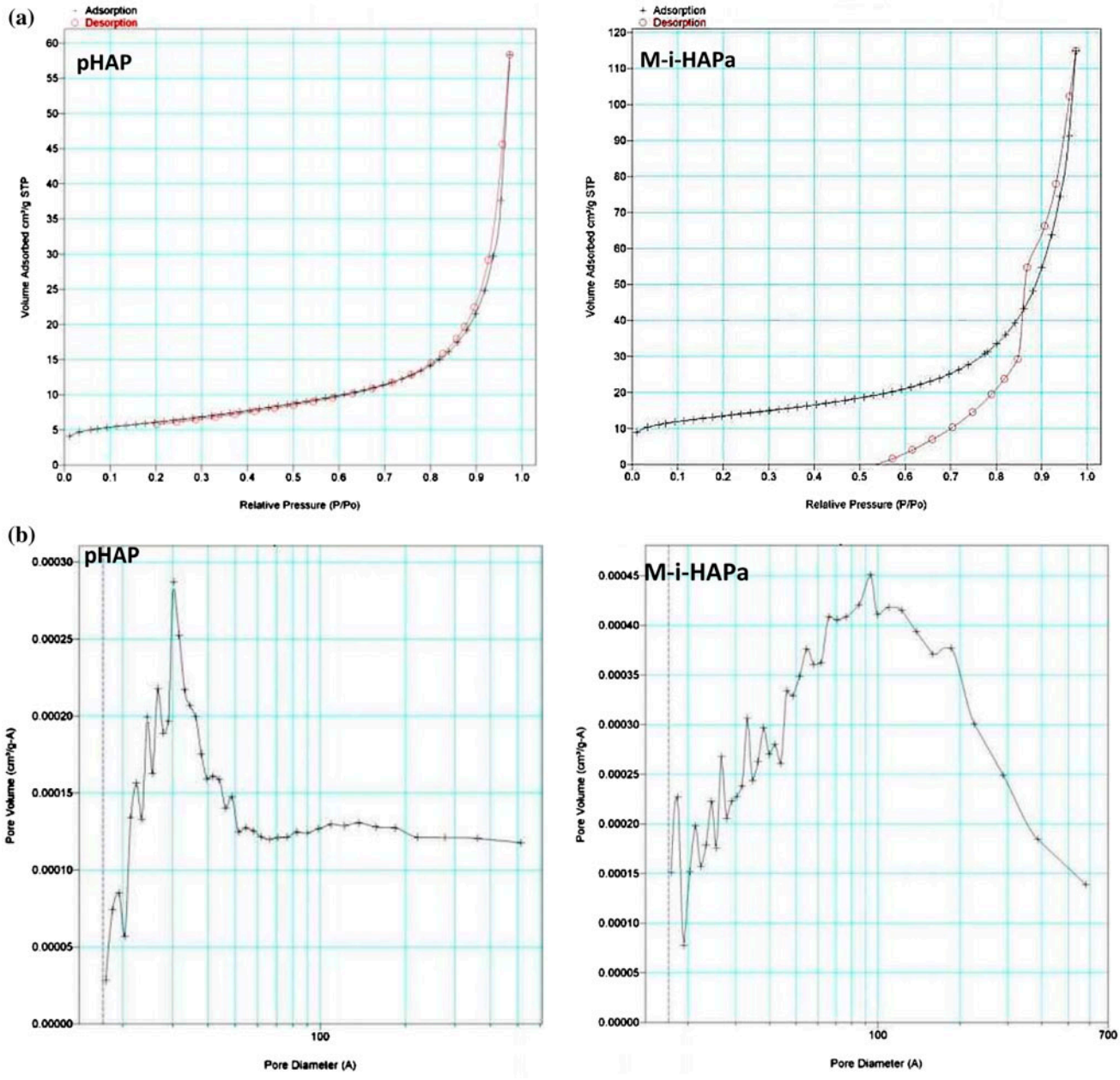

Fig. 2. (a) N_2 adsorption/desorption isotherm and (b) pore size distribution of pHAP and M-i-HAPa.

(10 mg/L) it was observed that more than 70% removal was achieved in the first 30 min itself. After 135 min, the removal rate started to stabilize with negligible removal after 180 min indicating attainment of equilibrium (Fig. 5(c)). The driving force for mass transfer between solid and liquid phases reduces with time and after exhaustion of the mesopores, fluoride ions have to encounter higher resistances which tend to slow adsorption at later stages.

3.5. Effect of initial fluoride concentration

The effect of fluoride concentrations (2–20 mg/L) on the fluoride removal was studied using a dosage of 10 g/L and is illustrated in Fig. 5(d). The results show that removal of fluoride decreased with increasing initial fluoride concentration and reached equilibrium at 10 mg/L. This may be due to the fact that for a fixed adsorbent dose, the total available adsorption sites are restricted, which became saturated at elevated concentration.

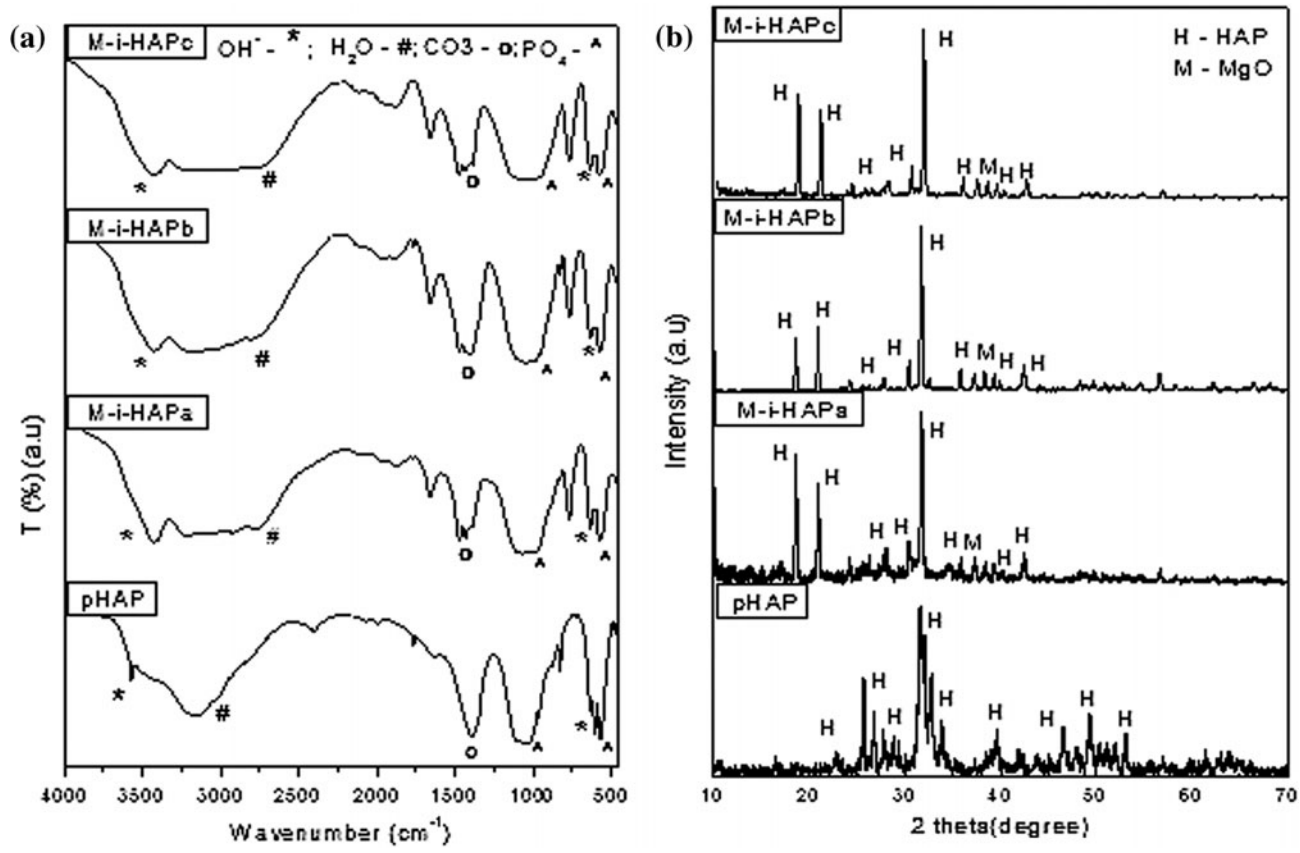

Fig. 3. Characterization of M-i-HAP: (a) FTIR spectra, (b) XRD, (c) TEM images, and (d) EDX pattern.

3.6. Effect of coexisting ions

Groundwater contaminated with fluoride contains many other ions which compete with fluoride during the adsorption process [3]. To examine the effect of these coexisting ions studies were conducted with varying concentrations (100–300 mg/L) of chloride, sulfate, nitrate, phosphate, and bicarbonate anions. It is clear from Fig. 5(e) that bicarbonate ions hinder the fluoride adsorption most prominently even at lower anion concentration. Chloride, sulfate, nitrate, and phosphate ions reduce the adsorbent capacity only at higher anion concentration (300 mg/L). This decrease in fluoride uptake capacity of M-i-HAP is attributed to the competition among the coexisting ions for the sites on the adsorbent surfaces which is governed by the charge, concentration, and size of the ion. The order of interference in terms of reduction in adsorption capacity posed by the coexisting ions is as follows: Chloride < Sulfate < Nitrate < Phosphate < Bicarbonate. Chloride, nitrate, and sulfate ions form outer sphere complexes, whereas phosphate and bicarbonate ions form inner sphere complexes with binding surfaces [34]. The adsorption mechanism for chloride, nitrate, and sulfate is through the formation of weak bonds with the sorption sites at the outer Helmholtz plane. Therefore, their presence in solution have less effect on adsorption of fluoride since fluoride ions interact via forming strong bonds with sorption sites at the inner Helmholtz plane. Phosphate and bicarbonate ions may also compete for active sorption site thus, reducing the fluoride uptake capacity of the adsorbent. The adverse effect on removal capacity due to presence of bicarbonate ions in solution was also recounted by Kamble et al. [35], Veeraputhiran and Alagumuthu [36], and Sakhare et al. [37].

3.7. Effect of temperature

The effect of temperature on fluoride removal was studied in the solution temperature range from 303 to 323 K. It showed that fluoride removal capacity of the M-i-HAPa decreased with the increase in temperature (Fig. 6). The lower removal capacity at high temperatures may attribute to the fact that at

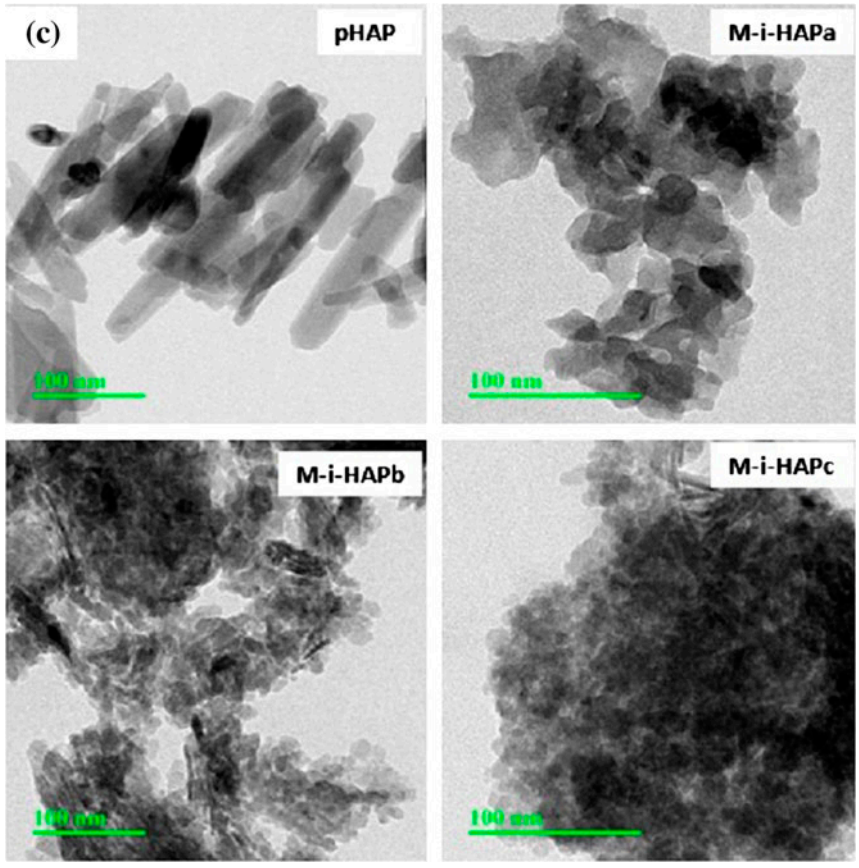

Fig. 3. (*Continued*).

higher temperatures the thickness of the boundary layer decreases due to increased tendency of the molecules to escape from the adsorbent surface to the solution phase, which results in a decrease in the adsorption capacity as temperature is increased [33,38]. In order to test the feasibility and spontaneity of the process, free energy change (ΔG°), enthalpy change (ΔH°), and entropy change (ΔS°) were calculated using Eqs. (5) and (6):

$$\Delta G^{\circ} = -RT \ln K_e \tag{5}$$

$$\ln K_e = \frac{\Delta S^{\circ}}{R} - \frac{\Delta H^{\circ}}{RT} \tag{6}$$

where K_e is the thermodynamic equilibrium and is expressed in Eq. (7):

$$K_e = \frac{C_{ae}}{C_e} \tag{7}$$

where C_{ae} and C_e equilibrium solute concentration (mg/L) on M-i-HAPa and solution, respectively.

The values of Gibbs free energy at 303, 313, and 323 K were found to be –7.15, –6.16, and –5.10 kJ/mol, respectively. The negative values of ΔG° confirm the spontaneous nature of adsorption of the fluoride ion by M-i-HAP, while the negative value of ΔH° (–38.13 kJ/mol) shows that the process is exothermic. The negative values of ΔS° (–0.102 kJ mol^{-1} K^{-1}) imply increased randomness at the solid-solution interface during the adsorption process [33].

3.8. Response surface methodological approach

3.8.1. Experimental design and quadratic model fitting

RSM was employed for fluoride removal using M-i-HAPa adsorbent and its process parameters were optimized. The relevance of this approach is based on an empirical relationship between input parameters and response generated which is stated by a quadratic model. The result obtained through each experimental run is presented in Table 1. After conducting different runs for design and statistical analysis, the final equation in terms of coded factors are shown in Eqs. (8) and (9):

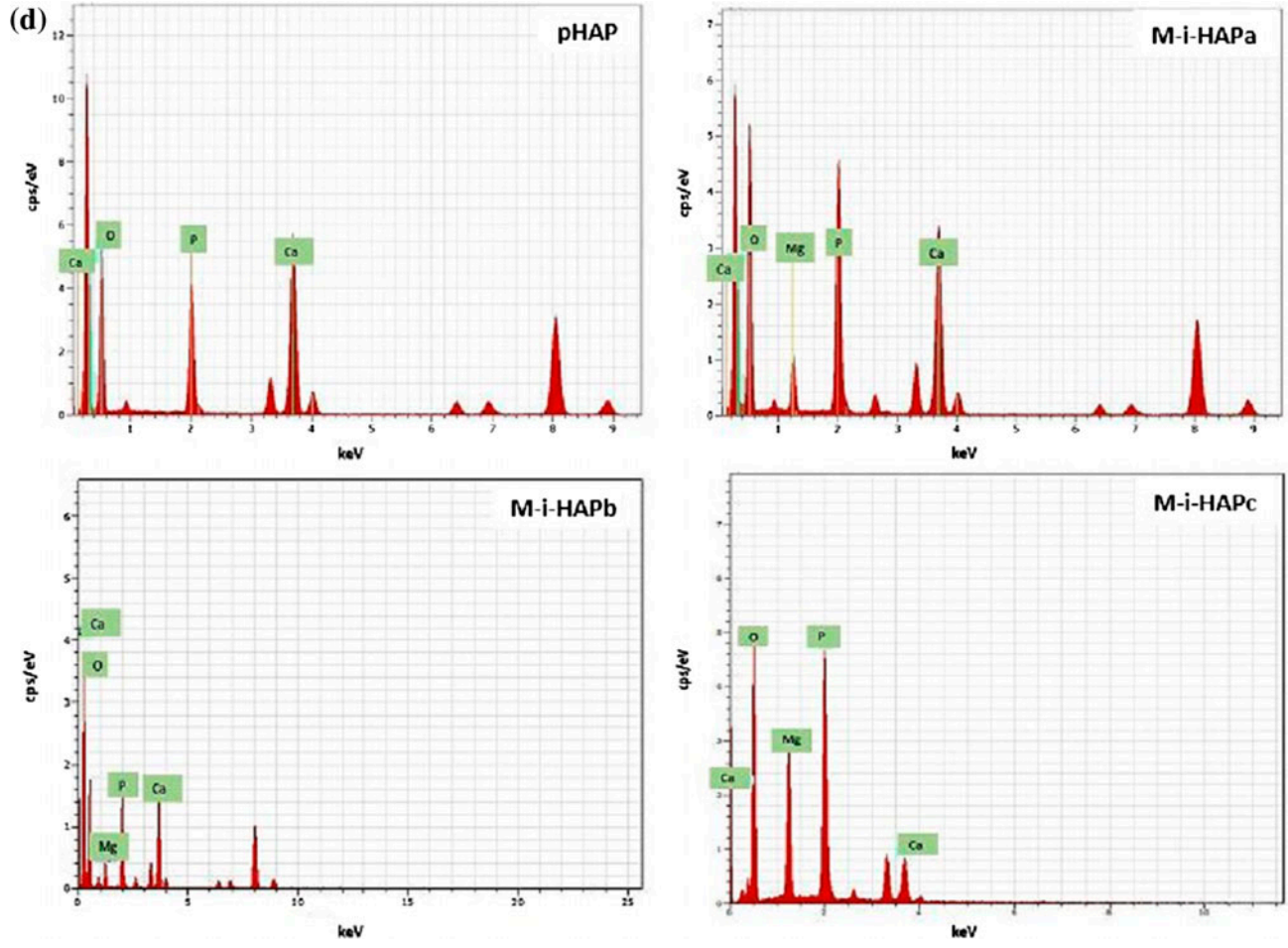

Fig. 3. (*Continued*).

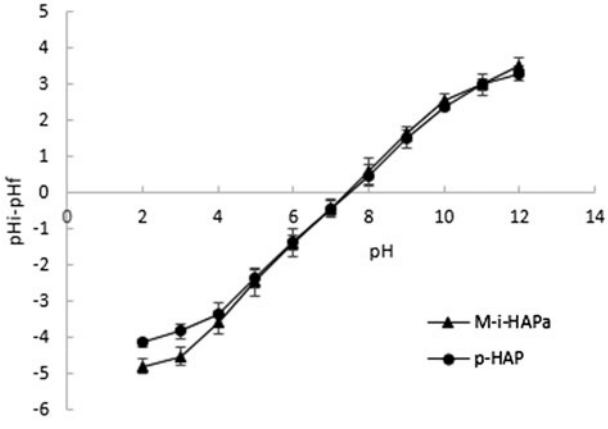

Fig. 4. pH_{PZC} determination for M-i-HAPa and pHAP.

$$\begin{aligned}\text{Fluoride removal }(\%) = {} & 90.12 + 19.44A - 4.12B \\ & + 10.83C - 1.36D + 0.88AB \\ & + 6.15625AC + 0.86AD \\ & - 1.88BC - 0.84BD + 0.30CD \\ & - 33.73A^2 + 0.35B^2 - 7.58C^2 \\ & + 2.66D^2\end{aligned} \tag{8}$$

$$\begin{aligned}&\text{Adsorption capacity (mg/g)} \\ &= 0.96 - 0.60A - 0.12B + 0.16C - 0.058D + 0.11AB \\ &\quad - 0.071AC + 0.05AD - 0.06BC - 0.04B - 0.006CD\end{aligned} \tag{9}$$

where *A*, *B*, *C*, and *D* are four independent variables. A positive sign for terms signify synergistic effect whereas a negative sign signifies antagonistic effects [32]. The outcome of the quadratic model for fluoride removal (%) and adsorption capacity (mg/g) in the form of analysis of variance (ANOVA) is presented in

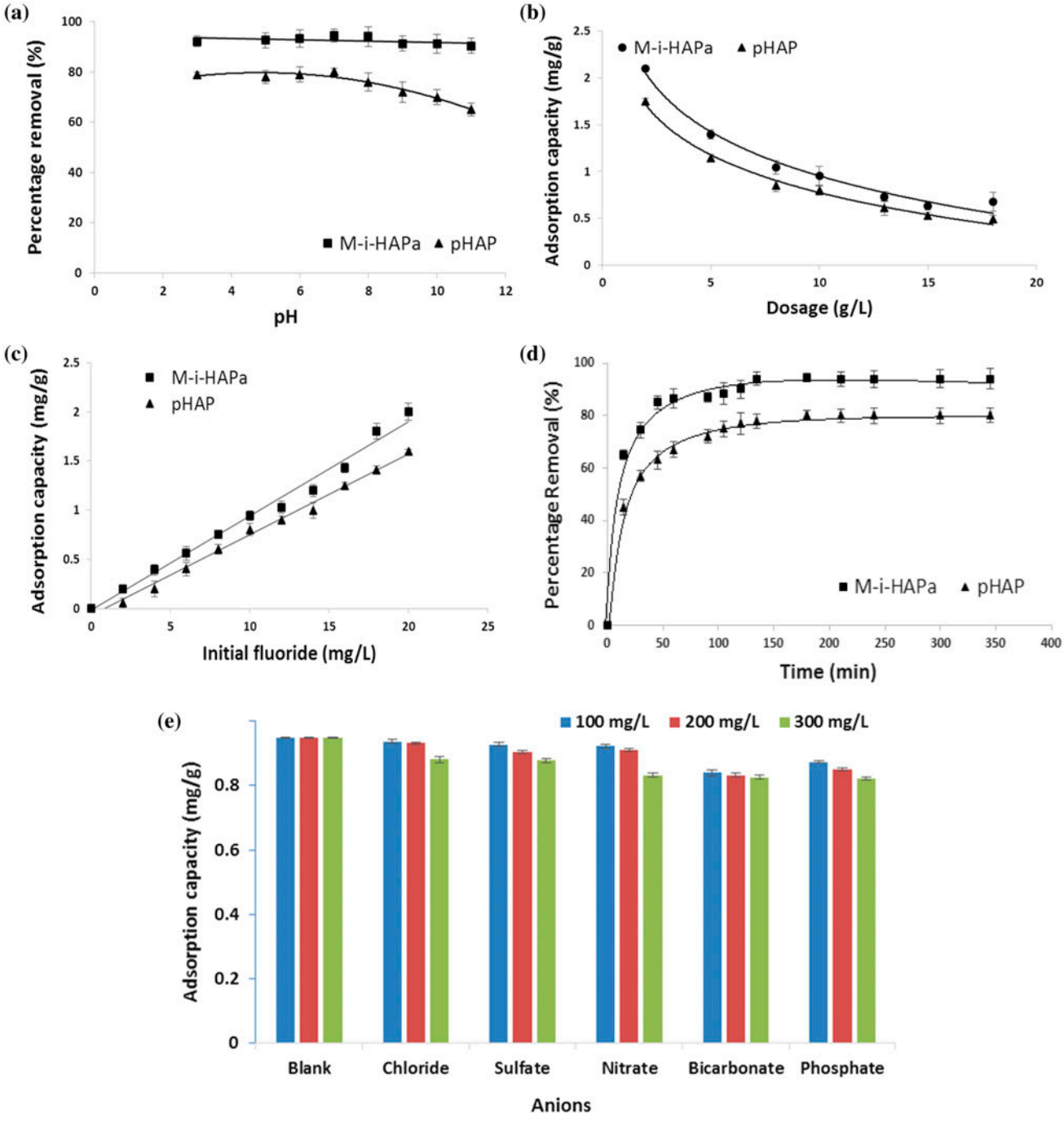

Fig. 5. Effect of various parameters: (a) pH, (b) adsorbent dose, (c) fluoride concentration, (d) contact time, and (e) coexisting ions.

Tables 2 and 3, respectively. It is observed that the value of correlation coefficient was 0.99 and 0.97, respectively for fluoride removal percentage and adsorption capacity with the respective standard deviation being 1.81 and 0.12. Additionally, the model *F*-value is also significant, while the model depicts extremely low value of pure error of 0.21–8.333 E-005 for fluoride removal percentage and adsorption capacity, respectively. This implies that the regression model provides a very good elucidation of the relationship between the independent variables (chosen factors) and the response. The plot of predicted values vs. experimental values for fluoride removal (%) and adsorption capacity (mg/g) is illustrated in Fig. 7(a)

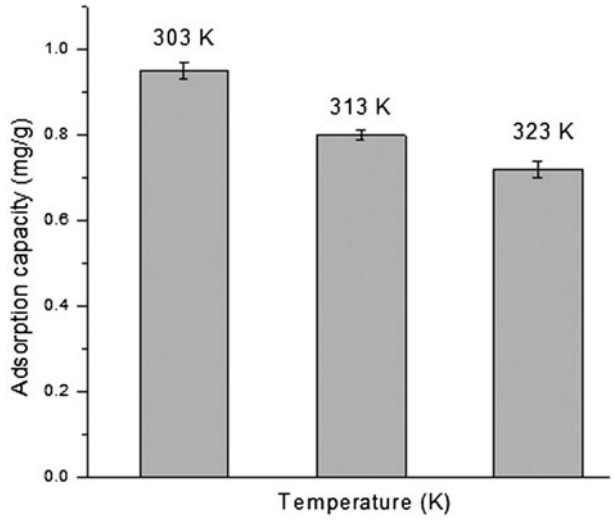

Fig. 6. Effect of temperature on fluoride removal capacity (Dose 10 g/L; pH 7; time 180 min).

and (b), respectively, indicating that the models developed were successful in estimating the correlation.

3.8.2. Effects of experimental factors on adsorption

For the graphical interpretation of the interactions, the use of three-dimensional plots of the regression model is vastly suggested [39]. The *F*-value in Tables 2 and 3 confirmed that all the four chosen factors have significant effect on the removal efficiency of fluoride. In order to assess the relationship between the experimental factors and responses, 3D response surface plots were generated and presented in Fig. 8 as graphical representations of the regression equation. The adsorption capacity of M-i-HAPa increased with elevated F^- concentration and contact time, and reduced slightly with increase in pH. However, the adsorbent worked considerably well over a wide range of pH. With increase in temperature, the fluoride removal efficiency was noticed to decrease, indicating an exothermic reaction.

3.8.3. Verification of the model and confirmatory experiments

The desired goal for each factor and response was selected in numerical optimization. Fig. 9 shows desirability ramp for numerical optimization. The variables were set within the studied range and goals were targeted to achieve maximum possible adsorption capacity and removal percentage by the software. The obtained value of desirability (1.000) showed that the estimated function may represent the experimental model and desired condition. For confirming the data as given by numerical modeling under optimized condition, the confirmatory experiments were conducted with the parameters as suggested by the model (pH 7, adsorbent dose 10 g/L, temperature 303 K, and contact time 180 min). The efficiency of fluoride removal

Table 2
Analysis of variance for percentage fluoride removal using M-i-HAPa

Source	Sum of squares	df	Mean square	*F*-value	*p*-value (Prob. > *F*)
Model	20,649.65	14	1,474.98	174.26	<0.0001
A-Adsorbent dose	6,175.07	1	6,175.07	729.55	<0.0001
B-Temperature	2,223.58	1	2,223.58	262.70	<0.0001
C-Time	2,133.71	1	2,133.71	252.09	<0.0001
D-pH	14.09	1	14.09	1.67	0.2164
AB	7.70	1	7.70	0.91	0.3553
AC	839.55	1	839.55	99.19	<0.0001
AD	1.05	1	1.05	0.12	0.7295
BC	32.21	1	32.21	3.80	0.0700
BD	2.98	1	2.98	0.35	0.5621
CD	4.31	1	4.31	0.51	0.4867
A^2	451.52	1	451.52	53.34	<0.0001
B^2	44.74	1	44.74	5.29	0.0363
C^2	2.62	1	2.62	0.31	0.5862
D^2	30.18	1	30.18	3.57	0.0785
Residual	126.96	15	8.46		
Lack of fit	126.91	10	12.69	1189.78	<0.0001
Pure error	0.053	5	0.011		
Cor total	20776.61	29			

Table 3
Analysis of variance for fluoride adsorption capacity using M-i-HAPa

Source	Sum of squares	df	Mean square	*F*-value	*p*-value (Prob. > *F*)
Model	7.17	10	0.72	52.54	<0.0001
A-Adsorbent dose	5.97	1	5.97	437.68	<0.0001
B-Temperature	0.27	1	0.27	19.79	0.0003
C-Time	0.43	1	0.43	31.84	<0.0001
D-pH	0.057	1	0.057	4.16	0.0555
AB	0.21	1	0.21	15.70	0.0008
AC	0.082	1	0.082	6.03	0.0238
AD	0.045	1	0.045	3.32	0.0841
BC	0.061	1	0.061	4.47	0.0480
BD	0.031	1	0.031	2.29	0.1463
CD	7.290E−004	1	7.290E−004	0.053	0.8197
Residual	0.26	19	0.014		
Lack of fit	0.26	14	0.019	1,111.24	<0.0001
Pure error	8.333E−005	5	1.667E−005		
Cor total	7.43	29			

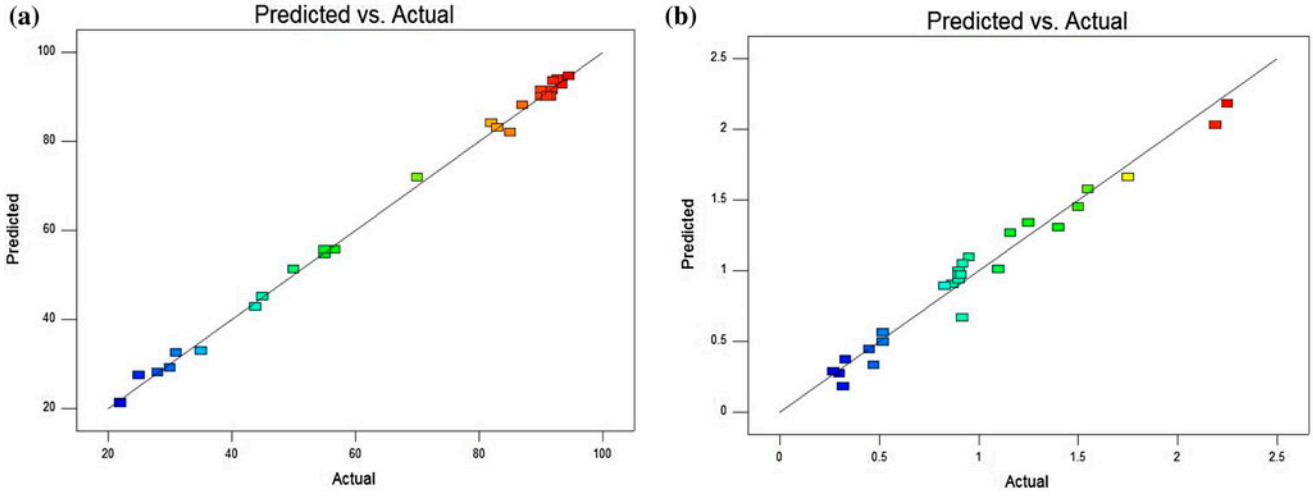

Fig. 7. Actual and predictive: (a) F^- removal % and (b) F^- removal capacity.

was found to be 94.5% and adsorption capacity was estimated to be 0.95 mg/g experimentally, while the model predicted it to be 94.6% and 1.09 mg/g, respectively. A good agreement was observed evidently between experimental and predicted values.

3.9. Adsorption isotherms

The data acquired during equilibrium study has been fitted to various adsorption isotherm equations such as Langmuir, Freundlich, Temkin, and Dubinin–Radushkevich (D–R) isotherms to gain insight of the equilibrium characteristics of the adsorption process. To identify the suitable isotherm for sorption of fluoride onto M-i-HAP the χ^2 analysis was carried out. It is assumed that smaller the χ^2 values, better the model fit with experimental data and vice versa. The mathematical expression in Eq. (10):

$$\chi^2 = \sum \frac{(q_{e,exp} - q_{e,calc})^2}{q_{e,calc}} \tag{10}$$

where $q_{e,calc}$ is the equilibrium capacity obtained by calculating from the model (mg/g) and $q_{e,exp}$ is the experimental data on the equilibrium capacity (mg/g).

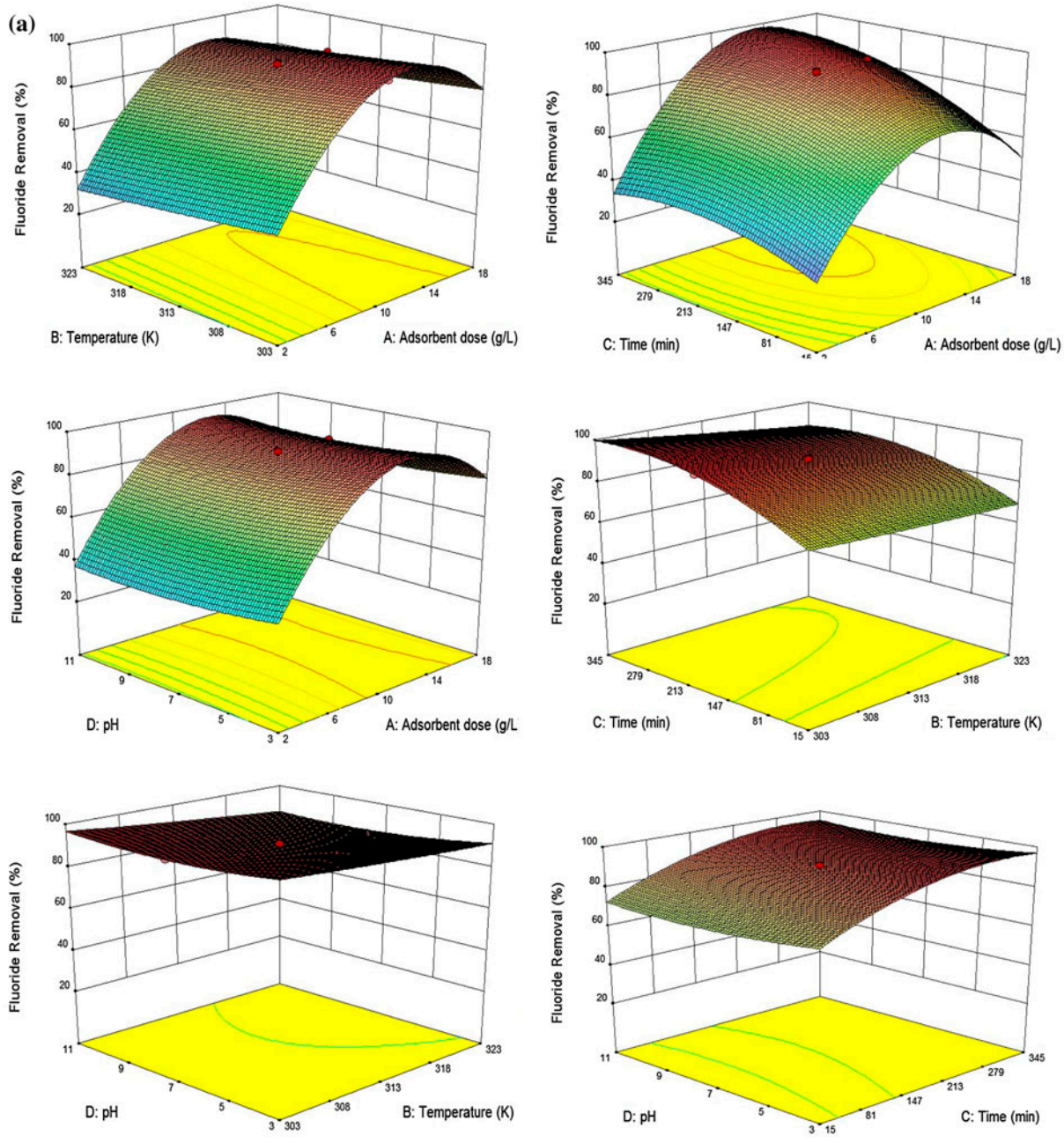

Fig. 8. Response surface plots for M-i-HAPa: (a) varying parameters for fluoride removal efficiency and (b) varying parameters for adsorption capacity.

The values of various parameters of the isotherms along with the mathematical equations are given in Table 4. The adsorption mechanism can be best described using Langmuir isotherm attributing to highest R^2 value of 0.99 and extremely low χ^2 value of 2.1E-3 (Table 4). This indicates uniform distribution of active sites on M-i-HAPa surface and a monolayer adsorption mechanism.

3.10. Kinetic study

Kinetic models recurrently used to determine various kinetic parameters of the adsorption system are reaction-based and diffusion-based models. For analyzing the reaction kinetics pseudo-first-order and pseudo-second-order models have been used. Diffusion models are employed for the adsorption of a

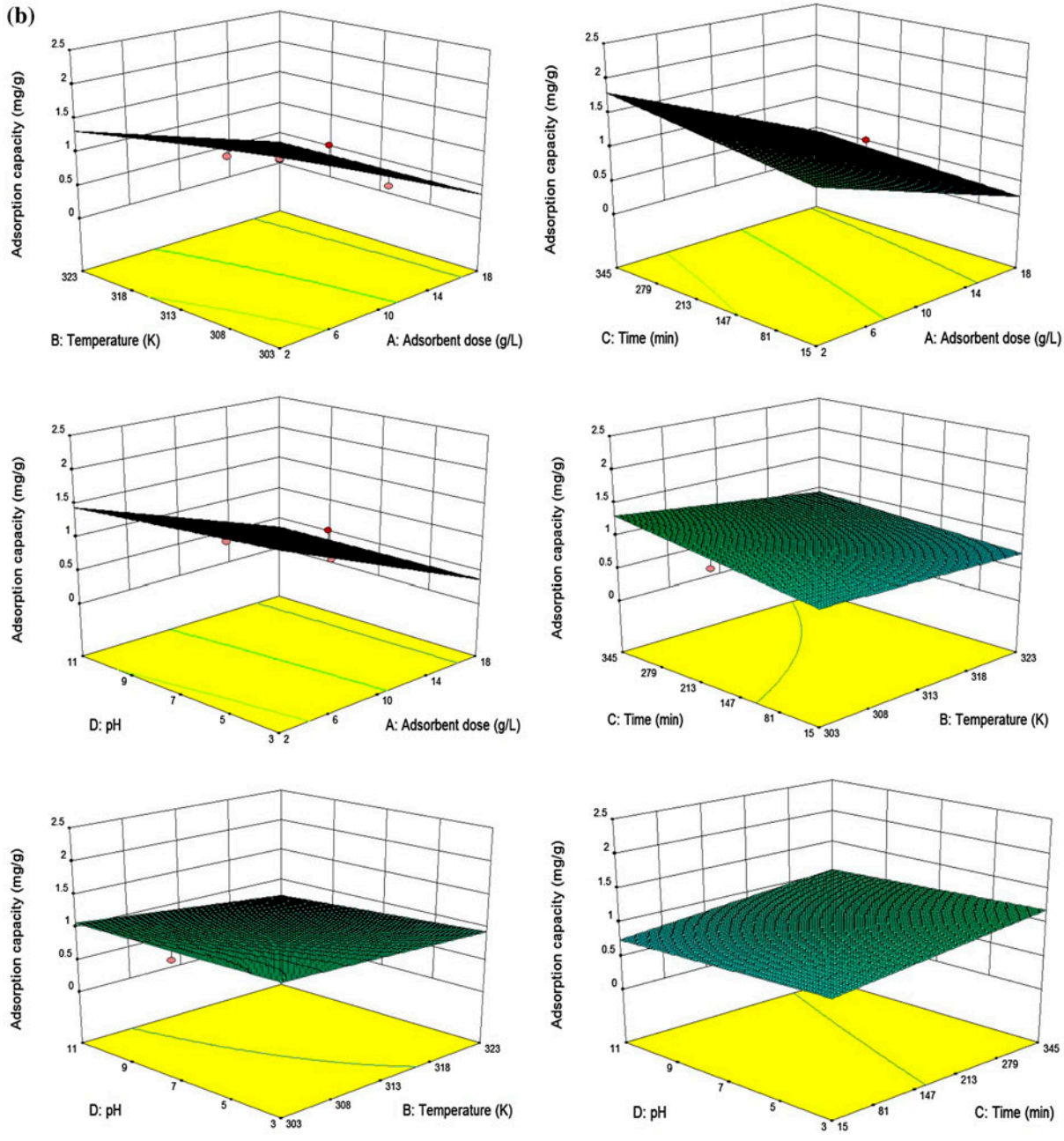

Fig. 8. (*Continued*).

liquid adsorbate on porous solid, which can be particle or pore diffusion model. For assessing best-fit among the kinetic models squared sum of errors squared (SSE) were evaluated and are expressed in Eq. (11):

$$\mathrm{SSE} = \sum \frac{(q_{t,\mathrm{exp}} - q_{t,\mathrm{calc}})^2}{q_{t,\mathrm{exp}}^2} \tag{11}$$

where $q_{t,\mathrm{exp}}$ and $q_{t,\mathrm{calc}}$ are the experimental sorption capacities of fluoride (mg/g) at time t and the corresponding values acquired from the kinetic models. The values of different kinetic model parameters with their mathematical expression are presented in Table 5 and it is apparent that pseudo-second-order kinetic model fits the best. Higher value of R^2 and lower SSE values point to the possibility of

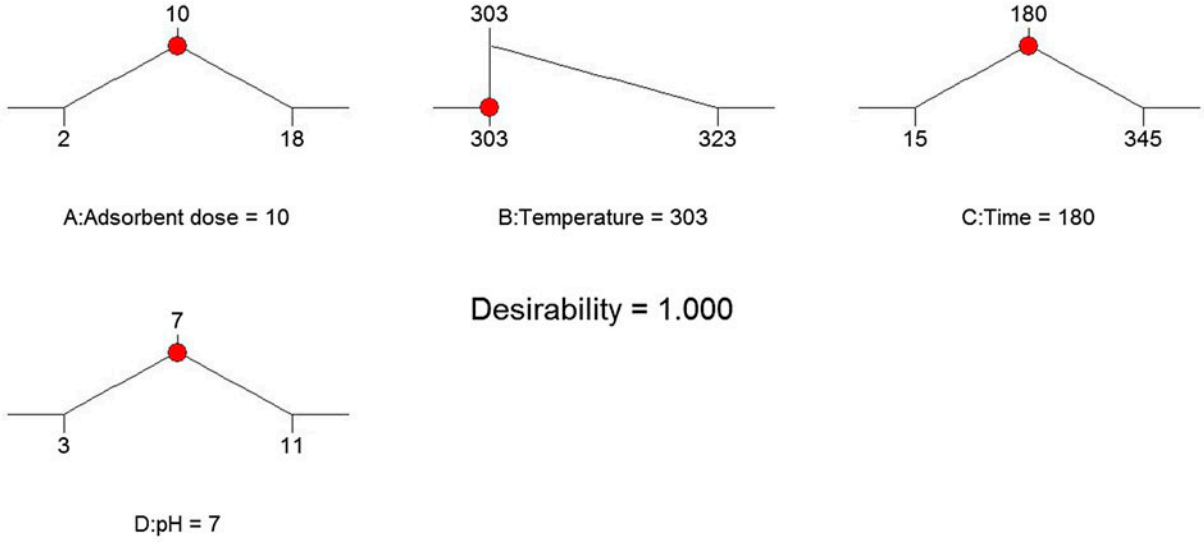

Fig. 9. Desirability ramp for numerical optimization.

Table 4
Adsorption isotherm parameters for fluoride adsorption onto M-i-HAPa

Isotherms	Parameters	303 K	313 K	323 K
Langmuir $\frac{C_e}{q_e} = \frac{1}{bQ_0} + \frac{C_e}{Q_0}$	$q_{e,exp}$ (mg/g)	0.95	0.8	0.72
	Q_o	1.16	1.17	0.79
	b (L/g)	5.9	1.16	2.21
	R^2	0.99	0.93	0.98
	K_{ap}	6.89	1.75	1.36
	χ^2	2.1E−3	0.024	0.153
Freundlich $\log q_e = \log K_f + \frac{1}{n} \log C_e$	n	4.14	2.65	2.25
	R^2	0.988	0.974	0.948
	K_f (mg/g)	0.857	0.572	0.519
	χ^2	0.074	0.320	0.279
Dubinin–Radushkevich $\ln q_e = \ln q_d - B\varepsilon^2$ where, $\varepsilon = RT \ln [1 + \frac{1}{C_e}]$	E (kJ/mol)	235.7	235.7	158.11
	R^2	0.806	0.748	0.741
	q_d (mg/g)	0.98	0.72	0.76
	χ^2	0.017	0.10	0.025
Temkin $q_e = B_T \ln A_T + B_T \ln C_e$	A_T (L/g)	81.45	6.56	24.9
	B_T	0.21	0.306	0.170
	R^2	0.918	0.964	0.946
	χ^2	0.10	0.25	0.31

contribution of intraparticle diffusion over pore diffusion in the process.

Table 6 shows a comparison between M-i-HAPa and adsorbents previously studied by various researchers and reported with their respective fluoride removal capacities. It was observed that M-i-HAPa was better than many adsorbents reported in literature.

3.11. Mechanism of fluoride adsorption

The adsorption mechanism of M-i-HAPa in aqueous fluoride solution was examined through XRD pattern obtained (Fig. 10) which illustrated the formation of hydroxyfluoropatite (034-0010) and fluorapatite (00-034-0011) as expected. The mechanism is further described through the following reactions in Eqs. (12) and (13):

Table 5
Kinetic model parameters for fluoride adsorption onto M-i-HAPa

Kinetic models	Parameters	303 K	313 K	323 K
Pseudo-first-order $\log(q_e - q_t) = \log q_e - \frac{b_1 t}{2.303}$	k_1 (min^{-1})	0.23	0.032	0.2
	R^2	0.705	0.803	0.70
	$q_{e,calc}$	0.406	0.595	0.40
	SSE	0.32	0.072	0.136
Pseudo-second-order $\frac{t}{q_t} = \frac{1}{b_2 q_e^2} + \frac{1}{q_e t}$	k_2 (g/mg min)	0.113	0.1	0.03
	R^2	0.997	0.966	0.986
	$q_{e,calc}$ (mg/g)	0.981	0.853	0.766
	SSE	1.38E−3	2.76E−3	2.70E−3
Intraparticle diffusion $q_t = k_i\, t^{1/2}$	k_i (mg/g $min^{0.5}$)	0.114	0.62	0.046
	R^2	0.933	0.988	0.812
	SSE	0.4	0.13	0.53
Particle diffusion $\ln \frac{C_t}{C_e} = -k_p t$	k_p (min^{-1})	0.11	0.009	0.007
	R^2	0.82	0.966	0.951
	SSE	0.72	0.31	0.76

Table 6
Fluoride removal capacity of some adsorbents in comparison with M-i-HAPa

Adsorbent	Refs.	Removal capacity (mg/g)
Modified immobilized activated alumina	[40]	0.76
Nano-Synthetic hydroxyapatite	[11]	0.48
Protonated chitosan beads	[41]	1.66
Calcite	[5]	0.39
Lignite	[42]	0.71
Kaolinite clay	[43]	0.045
Montmorillonite	[8]	0.263
Laterite	[44]	0.85
Chitin composite	[9]	0.29
Magnesium-incorporated hydroxyapatite	Present study	1.16

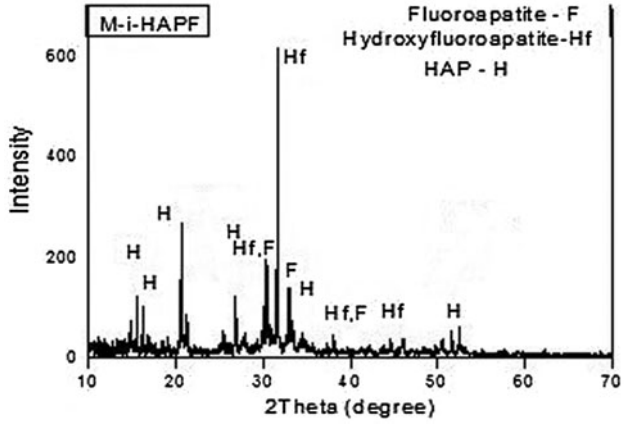

Fig. 10. XRD pattern of M-i-HAPa after fluoride adsorption (M-i-HAPF).

$$Ca_{(10-n)}\ Mg_n\ (PO_4)_6(OH)_2 + F^- \rightarrow Ca_{(10-n)}\ Mg_n\ (PO_4)_6(OH)\ (F) + OH^- \quad (12)$$

Magnesium-incorporated Hydroxyfluoroapatite

$$Ca_{(10-n)}\ Mg_n\ (PO_4)_6(OH)\ (F) + F^- \rightarrow Ca_{(10-n)}\ Mg_n\ (PO_4)_6\ F_2 \quad (13)$$

Magnesium-incorporated Fluoroapatite

Fluoride adsorption onto M-i-HAPa was accelerated at first then reached a stationary phase with increased contact time. Thus, the mechanism of fluoride adsorption involves diffusion of F^- ions on

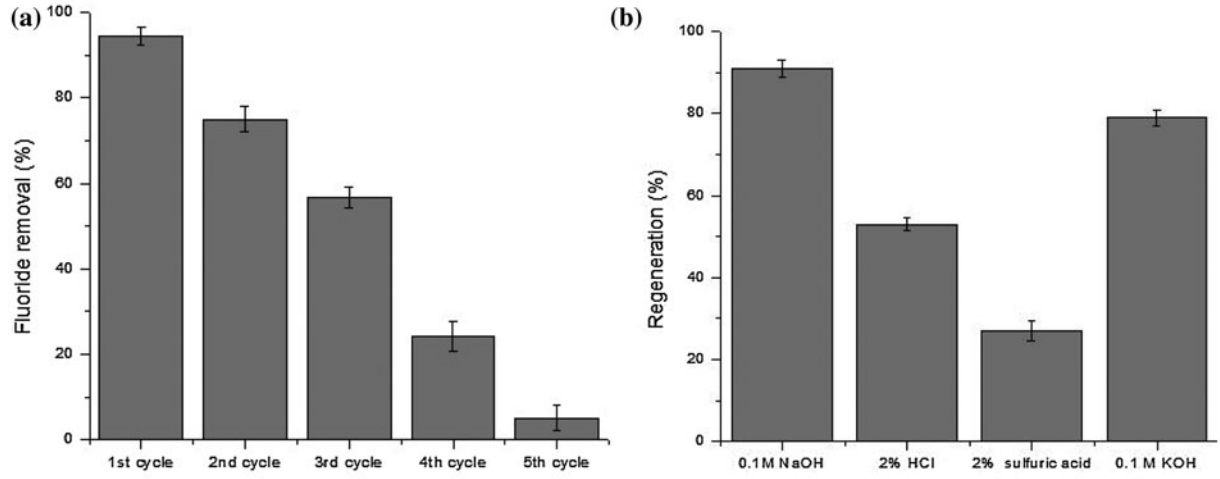

Fig. 11. (a) Reuse of adsorbent (F^- concentration: 10 mg/L) and (b) Regeneration studies.

Table 7
Treated water parameter analysis

	Before adsorption	After adsorption	Permissible limit
pH	7.54	7.32	6.5–8.5
EC (μS/cm)	67	502	Not mentioned
TDS (ppm)	33	248	500
Alkalinity ($CaCO_3$ eqv., mg/L)	0	15	600
Total Hardness ($CaCO_3$ eqv., mg/L)	0	135	500
Ca (mg/L)	0	20	75
Mg (mg/L)	0	27	30
Phosphate	0	Below detection limit	Not mentioned
F (mg/L)	10	0.552	1–1.5
Turbidity (NTU)	0	0	10

adsorbent surface then adsorption at active sites followed by exchange of OH^- and F^- ions.

3.12. Regeneration studies of M-i-HAPa

It is immensely essential to regenerate the saturated adsorbent to make the process cost-effective as well as to prevail over the disposal problem. The adsorbent was first saturated with fluoride solution of 10 g/L for 3 h and this cycle was repeated till M-i-HAPa got saturated (Fig. 11(a)). Approximately 20% decrease in removal efficiency was observed in the first two cycles followed by higher reduction in the efficiency in further cycles. The regeneration of adsorbent was studied using different solutions of sodium hydroxide, sulfuric acid, hydrochloric acid, and potassium hydroxide. The saturated adsorbent (10 g/L) was shaken with different regeneration solutions for 1.5 h after which it was filtered, washed, and dried at 95˚C for 1 h. The results obtained are illustrated in Fig. 11(b). About 91% regeneration was achieved with 0.1 M NaOH confirming to the ion exchange mechanism of adsorption.

3.13. Treated water quality analysis

The quality of water treated with M-i-HAPa adsorbent (dose: 10 g/L, contact time: 3 h) was studied for various parameters. Table 7 presents the value of concerned parameters before and after adsorption along with the permissible limit determined by WHO and BIS [1,2]. It is apparent from Table 7 that the water

treated with magnesium-incorporated hydroxyapatite is fit for consumption and all the parameters are within acceptable limit.

4. Conclusion

In this work, the adsorbent magnesium-incorporated hydroxyapatite was synthesized and investigated for fluoride removal. Characterization with XRD, FTIR, and TEM confirmed the incorporation of magnesium into the apatite lattice. BET surface area of the synthesized adsorbent was 46.62 m^2/g which is more than twice as compared to hydroxyapatite (21.25 m^2/g), due to this higher adsorption rate was attained. The influence of experimental factors (initial fluoride concentration, contact time, pH of the aqueous solution, dose of M-i-HAP, and temperature) on fluoride removal percentage was explored. RSM by CCD was used to investigate the chosen factors on fluoride removal and adsorption capacity. A second-order polynomial regression model interpreted the experimental data with coefficient of determination value of 0.99 and 0.97, respectively for fluoride removal percentage and adsorption capacity. The numerical optimization achieved with the desirability function specified the probable fluoride removal to be 94.60% and adsorption capacity to be 1.09 mg/g. The optimum values for experimental parameters were found to be pH 7, 303 K temperature, 10 mg/L fluoride concentration, and 180 min contact period with a dose of 10 mg/L. The mechanism of adsorption was governed by Langmuir model with maximum fluoride uptake of 1.16 mg/g. Pseudo-second-order kinetic model was followed by the process along with some contribution of intraparticle diffusion. Thermodynamic studies clearly show the spontaneity of the process and a better removal at lower temperatures. The adsorbent could be regenerated to 91% making the reusability of the adsorbent possible. Further, the M-i-HAPa treated water quality after defluoridation was tested as per drinking water standards and all the parameters such as TDS, pH, alkalinity, hardness, turbidity, EC, and residual ions (fluoride, phosphorus, calcium, and magnesium) were under permissible limits. Thus, the adsorbent M-i-HAPa is found to be surely a promising defluoridation agent.

Acknowledgements

The authors are thankful to Malaviya National Institute of Technology (MNIT) Jaipur, India for the financial support and Materials Research Centre, MNIT Jaipur for providing all the characterization facilities needed for this paper.

List of symbols

q_e — amount of adsorption at equilibrium (mg/g)
q_t — amount of adsorption at time t (mg/g)
C_i — initial concentrations of fluoride (mg/L)
C_e — equilibrium concentrations of fluoride (mg/L)
C_t — concentration of fluoride at time t (mg/L)
v — volume of the aqueous solution (L)
w — adsorbent mass (g)
Y — predicted response
b_0 — constant coefficient
b_i — linear coefficient
b_{ij} — interaction coefficient
b_{ii} — quadratic coefficient
X_i, X_j — coded values
Q_0 — maximum adsorption capacity reflecting complete monolayer (mg/g)
b — Langmuir constant related to energy
K_f — Freundlich constant (mg/g)
n — heterogeneity factor
R — universal gas constant (8.314 J/mol K)
T — temperature (K)
A_T — Temkin isotherm equilibrium binding constant (L/g)
B_T — Temkin isotherm constant
b_1 — adsorption rate constant of first order reaction (min^{-1})
b_2 — adsorption rate constant of first order reaction (g mg^{-1} min^{-1})
k_i — intraparticle diffusion rate constant (mg g^{-1} $min^{-1/2}$)
a — initial adsorption rate (mg g^{-1} min^{-1})
α — desorption rate (g mg^{-1})
B — Dubinin–Radushkevich isotherm constant
q_d — theoretical isotherm saturation capacity (mg/g)
ε — Polanyi potential
k_P — particle diffusion coefficient (min^{-1})

References

[1] World Health Organization, Guidelines for Drinking water Quality, Recommendations, Fourth ed., World Health Organization, Geneva, 2011.
[2] Indian Standard Drinking Water Specification, Bureau of Indian Standards, IS 10500, "Bureau of Indian" Standards, New Delhi, 2012.
[3] P. Mondal, S. George, A review on adsorbents used for defluoridation of drinking water, Rev. Environ. Sci. Biotechnol. 14 (2015) 195–210.
[4] Meenakshi, R.C. Maheshwari, Fluoride in drinking water and its removal, J. Hazard. Mater. 137 (2006) 456–463.
[5] X. Fan, Adsorption kinetics of fluoride on low cost materials, Water Res. 37 (2003) 4929–4937.
[6] S. Ghorai, K.K. Pant, Equilibrium, kinetics and breakthrough studies for adsorption of fluoride on activated alumina, Sep. Purif. Technol. 42 (2005) 265–271.

[7] P. Mondal, S. George, D. Mehta, Use of calcite for defluoridation of drinking water in acidic medium, Res. J. Chem. Sci. 4 (2014) 62–65.
[8] A. Tor, Removal of fluoride from an aqueous solution by using montmorillonite, Desalination 201 (2006) 267–276.
[9] J.L. Davila-Rodriguez, V.A. Escobar-Barrios, K. Shirai, J.R. Rangel-Mendez, Synthesis of a chitin-based biocomposite for water treatment: Optimization for fluoride removal, J. Fluorine Chem. 130 (2009) 718–726.
[10] C.S. Sundaram, N. Viswanathan, S. Meenakshi, Defluoridation chemistry of synthetic hydroxyapatite at nano scale: Equilibrium and kinetic studies, J. Hazard. Mater. 155 (2008) 206–215.
[11] S. Gao, R. Sun, Z. Wei, H. Zhao, H. Li, F. Hu, Size-dependent defluoridation properties of synthetic hydroxyapatite, J. Fluorine Chem. 130 (2009) 550–556.
[12] M. Jiménez-Reyes, M. Solache-Ríos, Sorption behavior of fluoride ions from aqueous solutions by hydroxyapatite, J. Hazard. Mater. 180 (2010) 297–302.
[13] G.E.J. Poinern, M.K. Ghosh, Y.-J. Ng, T.B. Issa, S. Anand, P. Singh, Defluoridation behavior of nanostructured hydroxyapatite synthesized through an ultrasonic and microwave combined technique, J. Hazard. Mater. 185 (2011) 29–37.
[14] C.M. Kanno, R.L. Sanders, S.M. Flynn, G. Lessard, S.C. Myneni, Novel apatite-based sorbent for defluoridation: Synthesis and sorption characteristics of nano-micro-crystalline hydroxyapatite-coated-limestone, Environ. Sci. Technol. 48 (2014) 5798–5807.
[15] Y. Nie, C. Hu, C. Kong, Enhanced fluoride adsorption using Al(III) modified calcium hydroxyapatite, J. Hazard. Mater. 233–234 (2012) 194–199.
[16] G. Tomar, A. Thareja, S. Sarkar, Enhanced fluoride removal by hydroxyapatite-modified activated alumina, Int. J. Environ. Sci. Technol. 12 (2014) 2809–2818.
[17] D. Mehta, S. George, P. Mondal, Synthesis of hydroxyapatite by chemical precipitation technique and study of its biodegradability, Int. J. Advent Technol. 2 (2014) 159–161.
[18] F. Ren, Y. Leng, R. Xin, X. Ge, Synthesis, characterization and *ab initio* simulation of magnesium-substituted hydroxyapatite, Acta Biomater. 6 (2010) 2787–2796.
[19] A. Farzadi, F. Bakhshi, M. Solati-Hashjin, M. Asadi-Eydivand, N.A. Abu Osman, Magnesium incorporated hydroxyapatite: Synthesis and structural properties characterization, Ceram. Int. 40 (2014) 6021–6029.
[20] P. Valerio, M.M. Pereira, A.M. Goes, M.F. Leite, The effect of ionic products from bioactive glass dissolution on osteoblast proliferation and collagen production, Biomaterials 25 (2004) 2941–2948.
[21] S.P. Kamble, S. Jagtap, N.K. Labhsetwar, D. Thakare, S. Godfrey, S. Devotta, S.S. Rayalu, Defluoridation of drinking water using chitin, chitosan and lanthanum-modified chitosan, Chem. Eng. J. 129 (2007) 173–180.
[22] X. Dou, Y. Zhang, H. Wang, T. Wang, Y. Wang, Performance of granular zirconium-iron oxide in the removal of fluoride from drinking water, Water Res. 45 (2011) 3571–3578.
[23] K.C. Agarwal, S.K. Gupta, A.B. Gupta, Development of new low cost defluoridation technology (krass), Water Sci. Technol. 40 (1999) 167–173.
[24] S. George, P. Pandit, A.B. Gupta, Residual aluminium in water defluoridated using activated alumina adsorption—Modeling and simulation studies, Water Res. 44 (2010) 3055–3064.
[25] Y. Zhang, B. Shi, Y. Zhao, M. Yan, D.A. Lytle, D. Wang, Deposition behavior of residual aluminum in drinking water distribution system: Effect of aluminum speciation, J. Environ. Sci. (2015), doi: 10.1016/j.jes.2015.05.010.
[26] M. Elibol, Response surface methodological approach for inclusion of perfluorocarbon in actinorhodin fermentation medium, Process Biochem. 38 (2002) 667–673.
[27] M.T. Tanyildizi, Modeling of adsorption isotherms and kinetics of reactive dye from aqueous solution by peanut hull, Chem. Eng. J. 168 (2011) 1234–1240.
[28] P. Ricou, I. Lecuyer, P. Le Cloirec, Influence of pH on removal of heavy metallic cations by fly ash in aqueous solution, Environ. Technol. 19 (1998) 1005–1016.
[29] W.L. Suchanek, K. Byrappa, P. Shuk, R.E. Riman, V.F. Janas, K.S. TenHuisen, Preparation of magnesium-substituted hydroxyapatite powders by the mechanochemical–hydrothermal method, Biomaterials 25 (2004) 4647–4657.
[30] American Public Health Association (APHA), Standard Methods for the Examination of Water and Wastewater. American Public Health Association, American Water Works Association, Water Environment Federation Publication, twenty-second ed., APHA, Washington, DC, 2012.
[31] I.A.W. Tan, A.L. Ahmad, B.H. Hameed, Adsorption of basic dye using activated carbon prepared from oil palm shell: Batch and fixed bed studies, Desalination 225 (2008) 13–28.
[32] D.C. Montgomery, Design and Analysis of Experiments, fifth ed., Wiley, New York, NY, 2007.
[33] R. Bhaumik, N.K. Mondal, Optimizing adsorption of fluoride from water by modified banana peel dust using response surface modelling approach, Appl. Water Sci. (2014) 1–21, doi: 10.1007/s13201-014-0211-9.
[34] A. Eskandarpour, M.S. Onyango, A. Ochieng, S. Asai, Removal of fluoride ions from aqueous solution at low pH using schwertmannite, J. Hazard. Mater. 152 (2008) 571–579.
[35] S.P. Kamble, P. Dixit, S.S. Rayalu, N.K. Labhsetwar, Defluoridation of drinking water using chemically modified bentonite clay, Desalination 249 (2009) 687–693.
[36] V. Veeraputhiran, G. Alagumuthu, Sorption equilibrium of fluoride onto *Phyllanthus emblica* activated carbon, Int. J. Res. Chem. Environ. 1 (2011) 42–47.
[37] N. Sakhare, S. Lunge, S. Rayalu, S. Bakardjiva, J. Subrt, S. Devotta, N. Labhsetwar, Defluoridation of water using calcium aluminate material, Chem. Eng. J. 203 (2012) 406–414.
[38] M.G. Sujana, S. Anand, Iron and aluminium based mixed hydroxides: A novel sorbent for fluoride removal from aqueous solutions, Appl. Surf. Sci. 256 (2010) 6956–6962.
[39] N. Aktaş, Optimization of biopolymerization rate by response surface methodology (RSM), Enzyme Microb. Technol. 37 (2005) 441–447.
[40] A.A. Rafique, M.A. Awan, A. Wasti, I.A. Qazi, M. Arshad, Removal of fluoride from drinking water using modified immobilized activated alumina, J. Chem. (2012), doi: 10.1155/2013/386476.

[41] N. Viswanathan, C.S. Sundaram, S. Meenakshi, Removal of fluoride from aqueous solution using protonated chitosan beads, J. Hazard. Mater. 161 (2009) 423–430.
[42] M. Pekař, Fluoride anion binding by natural lignite (South Moravian deposit of Vienna Basin), Water Air Soil Pollut. 197 (2008) 303–312.
[43] P.K. Gogoi, R. Baruah, Fluoride removal from water by adsorption on acid activated kaolinite clay, Indian J. Chem. Technol. 15 (2008) 500–503.
[44] M. Sarkar, A. Banerjee, P.P. Pramanick, A.R. Sarkar, Use of laterite for the removal of fluoride from contaminated drinking water, J. Colloid Interface Sci. 302 (2006) 432–441.